more coherent study. Details of experimental technique are also described in this reference.

[2]T. B. Reed, in *High Temperature Technology*, edited by N. K. Hiester (Butterworths, London, 1969), p. 655.

[3]L. J. van der Pauw, Philips Res. Rept. 13, 1 (1958).

[4]D. Watanabe, J. R. Castles, A. Jostens, and A. S. Malin, Acta Cryst. 23, 307 (1967).

[5]S. P. Denker, J. Appl. Phys. 37, 142 (1966).

[6]S. Takeuchi and K. Suzuki, J. Japan Inst. Metals (Sendai) 33, 279 (1969); 33, 284 (1969).

[7]P. Ehrlich, Z. Electrochem. 45, 362 (1939).

[8]M. D. Banus, T. B. Reed, M. Sjöstrand, and P. Keesom (unpublished).

[9]J. K. Hulm, C. K. Jones, R. Mazelsky, R. C. Miller, R. A. Hein, and J. W. Gibson, in *Low Temperature Physics*, edited by J. G. Daunt (Plenum, New York, 1965), p. 600.

[10]M. D. Banus, Mater. Res. Bull. 3, 723 (1968).

[11]N. J. Doyle, J. H. Hulm, C. K. Jones, R. C. Miller, and A. Taylor, Phys. Letters 26A, 604 (1968).

[12]J. M. Honig, W. E. Wahnsiedler, M. D. Banus, and T. B. Reed, J. Solid State Chem. 2, 74 (1970).

[13]E. R. Pollard, Ph. D. thesis (MIT, 1968) (unpublished).

[14]J. B. Goodenough, preceding paper, Phys. Rev. B 5, 2764 (1972).

PHYSICAL REVIEW B VOLUME 5, NUMBER 8 15 APRIL 1972

Determination of the Surface-Plasmon Dispersion Relation in Aluminum by Inelastic Electron Diffraction*

A. Bagchi
Department of Physics and Materials Research Laboratory, University of Illinois, Urbana, Illinois 61801
and The James Franck Institute, University of Chicago, Chicago, Illinois 60637

and

C. B. Duke
Department of Physics, Materials Research Laboratory and Coordinated Science Laboratory, University of Illinois, Urbana, Illinois 61801

(Received 8 December 1971)

Inelastic differential cross sections for low-energy ($10 \lesssim E \lesssim 10^3$ eV) electrons scattered from the (111) and (100) surfaces of aluminum are analyzed using a quantum field theory of inelastic processes. The analysis permits the determination of the dispersion relation and damping of excitations created by the electrons. For nominally clean Al(111), the surface-plasmon dispersion relation is found to be $\hbar\omega_s(p_\parallel) = 10.1 - 0.7p_\parallel + 10p_\parallel^2$, $10^{-2} \lesssim p_\parallel \lesssim 1$ Å^{-1}, for momenta measured in reciprocal angstroms and energies measured in electron volts. With this choice of the dispersion relation, the predictions of the theory also are in fairly good agreement with experimental inelastic scattering data from Al(100) surfaces. The accuracy of the method of analysis and possible improvements on it are discussed.

I. INTRODUCTION

Since the work of Ritchie[1] and Stern and Ferrell[2] establishing the existence of surface plasmons, their dispersion relation has interested both theorists and experimentalists. Surface plasmons are elementary excitations of a bounded electron gas. A study of their dispersion relation is useful for understanding the electronic properties of metal surfaces. For example, a knowledge of both the surface-plasmon dispersion relation and the electron–surface-plasmon coupling vertex is a necessary prerequisite to the construction of a theory[3] of the electron-metal interaction near the metal surface. The dispersion relation also may be important in a detailed theory of the processes of chemisorption and catalysis.

The surface-plasmon dispersion relation has been studied by Kanazawa[4] using an approximate quantum-mechanical theory, and by Ritchie and Marusak[5] in the hydrodynamic model. Microscopic derivations of this quantity have been given by Fedders[6] and Feibelman [7] who also studied surface-plasmon damping in the random-phase approximation (RPA). The full RPA integral equation for a surface-charge fluctuation recently has been solved[8,9] numerically to obtain the dispersion and damping of surface plasmons. Most theories predict a linear dependence of the surface-plasmon energy on its momentum $p_\parallel$ parallel to the surface, for small values of this quantity. (This result is valid in the limit that the effect of retardation, which is important for $p_\parallel \lesssim 10^{-3}$ Å^{-1}, can be ignored.) If we retain terms to second order in the momentum, then the energy and damping of surface plasmons may be written as

$$\hbar\omega_s(p_\parallel) = \hbar\omega_s + C_1 p_\parallel + C_2 p_\parallel^2 , \qquad (1)$$

$$\Gamma_s(p_\parallel) = \Gamma_s + D_1 p_\parallel + D_2 p_\parallel^2 . \quad (2)$$

Beck's RPA calculation[8] gives $C_1 \sim 4$ and $\Gamma_s = 0$. Bennett[10] developed a hydrodynamic model of surface-plasmon dispersion in which the coefficient of the linear term C_1 depends, both in magnitude and in sign, upon the electron-density profile near the surface.

Despite numerous measurements of electron energy-loss spectra associated with the excitation of surface plasmons, the dispersion relation of these plasmons is poorly known experimentally. Powell and Swan[11,12] originally detected surface plasmons by studying the energy-loss spectra of keV electrons reflected from surfaces of simple metals. Subsequently, surface-plasmon-induced losses have been measured by keV electron transmission, [13] optical techniques, [13–15] and low-energy-electron reflection. [16] However, the only reported measurement of the dispersion relation in the momentum range large compared to 10^{-3} Å^{-1} is that of Kunz[17] in magnesium. He finds for C_1 a small and negative value—a fact which can be rationalized using a hydrodynamic model, as shown by Bennett.[10]

Our objective in this paper is the determination of the dispersion relation of surface plasmons in aluminum in the region of $p_\parallel$ large compared to 10^{-3} Å^{-1}. Then we can neglect retardation effects and obtain information about the coefficients of the linear and the quadratic terms in Eq. (1). We extract this information from an analysis of experimental data on the diffraction of low-energy electrons accompanied by energy loss. Several authors[18–21] have emphasized the importance of inelastic low-energy-electron diffraction (ILEED) as a tool for investigating surface modes in a solid. The work of Duke and Laramore[18] is the most useful for our purpose because it exploits the diffraction nature of ILEED by introducing a two-step mechanism for scattering. Therefore their model permits us to identify the interesting ranges of energy for which we can utilize the measured inelastic scattering cross sections to determine the dispersion relation of surface plasmons. This feature is absent in single-step models of scattering because they do not permit the correlation of resonance maxima in the elastic and inelastic channels. The semiclassical theory of Lucas and Sunjić, [21] for example, says nothing about the fact that resonant elastic reflection makes inelastic processes appear prominent at certain energies which are simply related to the energies of maxima in the elastic scattering intensities. Also their model describes only the "total" inelastic cross section integrated over angles. Therefore, it is not directly useful for studying the surface-plasmon dispersion relation because the angular dependence of the intensity of the inelastically scattered electrons is the quantity which provides information about the dispersion of surface plasmons.

We proceed by analyzing experimental ILEED intensities for Al(111)[22,23] and Al(100). [24] In Sec. II we describe some refinements of the original theory of Duke and Laramore[18,19] used in our calculations. Our model predictions are compared with experimental data in Sec. III, in which we obtain values for the parameters of surface-plasmon dispersion and damping. In Sec. IV we summarize our results, indicate the limitations of the theory, and suggest possible ways of eliminating these limitations.

II. THEORY

The quantum field theory[18,19] of ILEED has been used to construct a model of two-step inelastic diffraction in which the diffraction of an electron by the lattice is followed by its energy loss to the solid or vice versa. The two-step mechanism for inelastic diffraction is well established experimentally, [22–26] and the amplitudes of the two processes should add coherently in accordance with the quantum theory of scattering. [18] Elastic diffraction of the electron by the lattice is described by the inelastic-collision model which has been discussed elsewhere. [27,28] For purposes of numerical calculation, we use the s-wave version of this model in which the electron–ion-core scattering is described by an angle-independent scattering amplitude,

$$t(E) = -h^2 \, (e^{2i\delta(E)} - 1)/4\pi ikm , \quad (3)$$

in which $\delta(E)$ is the s-wave phase shift of the presumed-identical aluminum ion-core scatterers. Both it and the other parameters[27,28] (i. e., an inner potential V_0 and inelastic-collision penetration depth λ_{ee}) associated with *elastic* electron-solid scattering are chosen to describe the measured[22–24] elastic low-energy-electron diffraction intensities.

The electron's energy loss results from its interaction with boson fields which may represent either surface or bulk plasmons. We can speak of the loss processes as independent because the various normal modes of a metal obey an orthogonality condition, [3,7] thus permitting us to add up their separate contributions to the scattering cross section.

The loss processes can be specified by the loss-mode dispersion relations and their coupling vertices to the electrons. It is convenient[18] to display this information in the form of the loss-mode spectral density $\Lambda_\alpha(n, m, \omega)$ defined in Eq. (2. 9) in the first of Refs. 18. Here α designates the type of boson field, whereas m and n are indices labeling the scattering planes. For the case of surface plasmons the spectral density can be written as

$$\Lambda_s(n, m, \omega) = -\sum_{\vec{p}_\parallel} t_s^*(\vec{p}_\parallel)\, t_s(\vec{p}_\parallel)\, e^{-i\vec{p}_\parallel \cdot (\vec{R}_m - \vec{R}_n)}$$

$$\times e^{-p_{\parallel}(|R_{m\perp}|+|R_{n\perp}|)} N(-w)\, 2i\, \mathrm{Im} D_s(\vec{p}_{\parallel}, \omega) , \quad (4)$$

in which $t_s(\vec{p}_{\parallel})$ is the vertex function, $D_s(\vec{p}_{\parallel}, \omega)$ the plasmon propagator, $\vec{R}_m$ and $\vec{R}_n$ the location of scattering centers, and $N(\omega)$ the Bose distribution function,

$$N(\omega) = (e^{\hbar\omega/\kappa T} - 1)^{-1} . \quad (5)$$

The vertex function that we use is[3,18]

$$t_s(\vec{p}_{\parallel}) = [(\pi e^2 \hbar\omega_s/p_{\parallel})\,\Omega^2]^{1/2}\,\theta(p_{cs} - p_{\parallel}) . \quad (6)$$

Here Ω is the volume of a unit cell and p_{cs} the momentum above which surface plasmons are not defined. The boson propagator is given by

$$D_s(\vec{p}_{\parallel}, \omega) = [\hbar\omega - \hbar\omega_s(p_{\parallel}) + i\,\Gamma_s(p_{\parallel})]^{-1} - [\hbar\omega + \hbar\omega_s(p_{\parallel}) + i\,\Gamma_s(p_{\parallel})]^{-1} , \quad (7)$$

where $\hbar\omega_s(p_{\parallel})$ and $\Gamma_s(p_{\parallel})$ are given by Eqs. (1) and (2).

For the excitation of bulk plasmons we use the coherent coupling vertex in semi-infinite jellium as given by Gersten.[3,29] The loss-mode spectral density is

$$\Lambda_b(n, m, \omega) = -\sum_{\vec{p}} t_b^*(\vec{p})\, t_b(\vec{p})\, e^{-i\vec{p}_{\parallel}\cdot(\vec{R}_m - \vec{R}_n)} \times 2\sin(p_{\perp}R_{m\perp})\sin(p_{\perp}R_{n\perp})\, N(-\omega)\, 2i\, \mathrm{Im}\, D_b(\vec{p}, \omega) , \quad (8)$$

where the solid is assumed to occupy all space for $z > 0$ and the vertex function is

$$t_b(\vec{p}) = -i\,[(\pi e^2 \hbar\omega_b/p^2)\,\Omega^2]^{1/2}\,\theta(p_{cb} - p) , \quad (9)$$

with p_{cb} denoting a cutoff in momentum. The bulk-plasmon propagator is

$$D_b(\vec{p}, \omega) = [\hbar\omega - \hbar\omega_b(p) + i\Gamma_b(p)]^{-1} - [\hbar\omega + \hbar\omega_b(p) + i\Gamma_b(p)]^{-1} , \quad (10)$$

and the plasmon dispersion relation is, to $O(p^2)$,

$$\hbar\omega_b(p) = \hbar\omega_b + Ap^2 , \quad (11)$$

while its damping is given by

$$\Gamma_b(p) = \Gamma_b + B_1 p^2 + B_2 p^4 . \quad (12)$$

The original theory[18,19] of electron-solid scattering has been modified in three important ways. First, we eliminate the restriction, imposed previously on sums over atomic layers, that the layer at which electronic loss processes occur lies closer to the surface than the layer where elastic diffraction takes place. In the double sum over layers performed in Appendix A of the first of Refs. 18, the elastic vertex sites (labeled by ν_2) are assumed to lie deeper into the solid than the loss vertex sites (labeled by ν_1). The restriction is unphysical because it ignores the possibility of backscattering of an electron losing energy to the boson field. We therefore allow the sum over ν_2 to go from zero to infinity. Secondly, we include the interaction of the incoming electron with the surface-plasmon field outside as well as inside the metal. As was pointed out in Refs. 18, this interaction is needed to recover the well-known results of Stern and Ferrell[2] from the vertex of Eq. (6). The precise statement of this extension of Duke and Laramore's model is obtained by altering Eq. (A1) in the first of Refs. 18 to read

$$S_1 = d \sum_{\nu_1=-\infty}^{\infty} e^{ik'_{\perp}d\nu_1} \sum_{\nu_2=0}^{\infty} e^{ik_{\perp}d\nu_2 - i\vec{g}\cdot\vec{a}_2}\, e^{ikd|\nu_2-\nu_1|} . \quad (13)$$

The details of the way in which the scattering cross section is modified are shown in the Appendix. We encounter a theoretical problem here with regard to the inelastic-collision damping of the electron wave field. The theory of inelastic scattering[18] is set up for plane-wave electrons, and they are not the eigenstates of a half-space, complex Hartree potential which describes a metal. This causes no problem so long as the electron is either wholly inside or wholly outside the metal. All that is involved then is the shifting of the zero level of energy. The situation is more complicated when the same electron interacts with a boson field both inside and outside the solid. We resolve the difficulty by taking the electronic momentum to be real outside the metal and complex inside. No such problem exists for the interaction of electrons with bulk plasmons because, for the sharp-junction jellium model that we are considering, the bulk-plasmon field does not extend outside the metal.[3]

The final change that we make in Duke and Laramore's model is the inclusion of a momentum-independent term in the damping of both surface and bulk plasmons. The existence of a finite, constant term Γ_b in bulk-plasmon damping is well known experimentally.[30] Our analysis of ILEED data leads us to conclude that Γ_s is also finite. The straightforward introduction of a finite, momentum-independent term in $\Gamma_b(p)$ or $\Gamma_s(p_{\parallel})$ leads to unphysical divergences of electronic cross section in the Duke-Laramore theory when $\vec{p}$ (or $\vec{p}_{\parallel}$) goes to zero. In the absence of a microscopic scattering theory for dissipative media, we take $p_{\parallel} \to [p_{\parallel}^2 + (\Gamma_s/C_1)^2]^{1/2}$ and $p \to (p^2 + \Gamma_b/A)^{1/2}$ in Eqs. (6) and (9) to estimate the effects of electron damping. This avoids unphysical divergences in line shapes while preserving the interesting features of the model predictions.

Once these changes have been incorporated in the theory, it is still straightforward[18] to work out inelastic cross sections for a single plasmon emission. Let (E, θ, ψ) be the energy, polar angle, and azimuthal angle of the incident electron and (E', θ', ψ') the same quantities for the scattered

electron. Let $\vec{k}$ and $\vec{k}'$ denote the electron momenta before and after scattering, their components parallel to the surface being given by $\vec{k}_{\parallel}$ and $\vec{k}'_{\parallel}$, respectively. We define the normal component of electron momentum inside the metal after diffraction as

$$k_{\perp}(\vec{g}, E) = \{2m[E - \Sigma(E)]/\hbar^2 - (\vec{k}_{\parallel} + \vec{g})^2\}^{1/2}, \quad (14)$$

where $\Sigma(E)$ is the complex electronic self-energy inside the metal. The form of $\Sigma(E)$ that we use is the same as in Refs. 18, viz.,

$$\Sigma(E) = -V_0 - i\Gamma(E), \quad (15a)$$

$$\Gamma(E) = \frac{\hbar^2}{m\lambda_{ee}}\left(\frac{2m}{\hbar^2}(E + V_0)\right)^{1/2}, \quad (15b)$$

where V_0 is the inner potential and λ_{ee} is, by definition, twice the inelastic-collision mean free path of an electron. The reciprocal-lattice vector $\vec{g}$ defines the order of the diffracted beam. The normal component of electron momentum outside the metal, $\tilde{k}_{\perp}(\vec{g}, E)$, is defined similarly to $k_{\perp}(\vec{g}, E)$ in Eq. (14), but with $\Sigma(E)$ set equal to zero. If we write w ($\equiv E - E'$) as the energy loss, then the differential scattering cross section for the two-step inelastic scattering of electrons by the surface-plasmon field is given by [cf. Eqs. (4.16) of the first of Refs. 18 and the Appendix]

$$\left(\frac{d^2\sigma}{d\epsilon\, d\Omega}\right)^{(4)}_{sp} = \left(\frac{E-w}{E}\right)^{1/2}\left(\frac{2\pi m}{h^2}\right)\frac{m\pi e^2\hbar\omega_s}{h^2}\frac{\Omega^2}{A} \times \sum_{\vec{g}} \frac{1}{[p_{\parallel}^2 + (\Gamma_s/C_1)^2]^{1/2}} \frac{2\Gamma_s(p_{\parallel})}{[w - \hbar\omega_s(p_{\parallel})]^2 + [\Gamma_s(p_{\parallel})]^2} |A'_b(\vec{g}, E) + A'_c(\vec{g}, E - w)|^2, \quad (16)$$

$$\vec{p}_{\parallel} = \vec{k}'_{\parallel} - \vec{k}_{\parallel} - \vec{g}, \quad (17)$$

$$A'_b(\vec{g}, E) = -\frac{imt(E)}{\hbar^2 A k_{\perp}(\vec{g}, E)} \{1 - \exp\{i(k_{\perp}[0, E] + k_{\perp}[\vec{g}, E])\, d - i\vec{g}\cdot\vec{a}\}\}^{-1} \times \left(\frac{1}{p_{\parallel} d + i(k'_{\perp}[0, E - w] - \tilde{k}_{\perp}[\vec{g}, E])\, d} + \frac{1}{1 - \exp\{i(k'_{\perp}[0, E - w] + k_{\perp}[0, E])\, d - p_{\parallel} d - i\vec{g}\cdot\vec{a}\}}\right), \quad (18)$$

$$A'_c(\vec{g}, E - w) = -\frac{imt(E - w)}{\hbar^2 A k'_{\perp}(-\vec{g}, E - w)} \{1 - \exp\{i(k'_{\perp}[0, E - w] + k'_{\perp}[-\vec{g}, E - w])\, d - i\vec{g}\cdot\vec{a}\}\}^{-1} \times \left(\frac{1}{p_{\parallel} d + i(\tilde{k}_{\perp}[0, E] - \tilde{k}'_{\perp}[-\vec{g}, E - w]\, d)} + \frac{1}{1 - \exp\{i(k_{\perp}[0, E] + k'_{\perp}[0, E - w])\, d - p_{\parallel} d - i\vec{g}\cdot\vec{a}\}}\right). \quad (19)$$

In Eqs. (16)–(19), A is the area of a unit cell, d the spacing between atomic layers, and $\vec{a}$ the vector displacement of a unit cell from one layer to the next.

The differential scattering cross section for the two-step inelastic scattering of electrons by the bulk-plasmon field is given by a formula very similar to Eq. (4.17a) of the first of Refs. 18. That equation must be multiplied by a factor of 2 to correct for a normalization error in going from plane-wave to sine-wave basis functions. The singular vertex has to be modified also before we can introduce a finite Γ_b. The final result is

$$\left(\frac{d^2\sigma}{d\epsilon\, d\Omega}\right)^{(4)}_{bp} = \left(\frac{E-w}{E}\right)^{1/2}\left(\frac{2\pi m}{h^2}\right)\frac{m\pi e^2\hbar\omega_b}{h^2}\frac{\Omega^2}{A}\sum_{\vec{g}}\int \frac{dp_{\perp}}{\pi}\frac{1}{p_{\parallel}^2 + p_{\perp}^2 + \Gamma_b/A}\frac{\Gamma_b(\vec{p}_{\parallel}, p_{\perp})}{[w - \hbar\omega_b(\vec{p}_{\parallel}, p_{\perp})]^2 + [\Gamma_b(\vec{p}_{\parallel}, p_{\perp})]^2} \times M[k_{\perp}(0, E), k'_{\perp}(0, E - w), p_{\perp}, \vec{g}]\, |A_b(\vec{g}, E) + A_c(\vec{g}, E - w)|^2, \quad (20)$$

where $\vec{p}_{\parallel}$ is given by Eq. (17), A_b and A_c are defined by Eqs. (4.16c) and (4.16e) in the first of Refs. 18, and we use, for the M function, the formula for coherent coupling, viz., Eq. (4.17c) of the first of Refs. 18. The complete differential cross section of an electron losing an energy w is given by a simple superposition of the contributions of Eqs. (16) and (20). In Sec. III we compare the predictions of our model with experimental ILEED intensities from Al(111)[22,23] and Al(100)[24] surfaces.

III. COMPARISON WITH EXPERIMENT

The principal conclusion of the analysis which we present below is that if the electron-plasmon vertex functions are known, a comparison between our model predictions and experimental data can

be utilized to determine the parameters in Eqs. (1) and (2) for the dispersion and damping of surface plasmons. It is convenient for this purpose to study the specular (00) beam on which ILEED measurements have been done[22,23] for electrons incident on Al(111) surface at an angle of 15°. Our analysis of the data has already been briefly reported elsewhere.[31] The various coefficients appearing in Eqs. (1), (2), (11), and (12) are regarded as parameters in the theory, to be obtained via a comparison with experiments. In principle, we can evaluate the parameters for bulk-plasmon dispersion relation and damping. However, the broad ILEED profiles give less reliable values for these numbers than those obtained from high-energy transmission experiments. Accordingly, we take the parameters describing the bulk-plasmon dispersion and damping from keV electron transmission data.[30,32] We use $A = 3.048$ eV Å^2, $\Gamma_b = 0.53$ eV, $B_1 = 0.103$ eV Å^2, and $B_2 = 1.052$ eV Å^4. For the bulk-plasmon threshold, however, the ILEED data require the use of $\hbar\omega_b = 14.2 \pm 0.2$ eV and not the value of 15 eV found in most high-energy experiments.[32,33] We cannot explain this discrepancy. However, it seems relevant to observe that Kunz[34] has reported 14-eV thresholds for certain thin films in his transmission experiments.

Our procedure for analyzing the experimental data is the following. The energy, polar angle, and azimuthal angle of the incident (E, θ, ψ) and the scattered (E', θ', ψ') beams are the six independent variables available in the experiments. It is convenient[18,35] in the theory to discuss either experiments which keep the angle of emergence (θ', ψ') fixed and study the intensity of scattered electrons as a function of the loss energy $w = E - E'$ (the "loss profile"), or those which keep the loss energy w fixed and study the intensity as a function of the angle θ' (the "angular profile"). We analyze the experimental data in the range $10 < E < 200$ eV of the primary beam energy and consider losses occurring in the range $5 \lesssim w \lesssim 20$ eV. The elastic electron-lattice scattering is described by the s-wave limit of the inelastic-collision model.[27,28] Detailed studies[18,35,36] of ILEED from aluminum indicate that within this model the analysis of elastic scattering in the first Born approximation (kinematic model) gives an adequate qualitative description of experiments. Therefore, as implied by Eqs. (18)–(20), we ignore multiple scattering processes and use the kinematical approximation to describe the elastic scattering vertices. The electron–ion-core scattering is specified by an energy-independent s-wave shift $\delta(E) = \frac{1}{4}\pi$, in Eq. (3), mainly to facilitate numerical computation. Within the context of the kinematical approximation for the elastic electron-solid scattering vertex, we repeated our analysis of the Al(111) data using a four-phase-shift APW model of the elastic electron-aluminum ion-core scattering. The three-phase-shift version of this model has been employed by Laramore *et al.*[37,38] in their detailed analysis of elastic low-energy-electron diffraction from the (100), (110), and (111) faces of aluminum. The sole effect of this extension of the analysis was a nearly uniform increase in all of the inelastic cross sections by a factor of about 4. The calculated line shapes and plasmon-dispersion relations were unaltered. Therefore, the s-wave approximation to the electron–ion-core elastic scattering vertex, used in constructing the figures and tables given herein, does not generate any additional uncertainties in the values of the parameters in Eqs. (1) and (2) extracted from the experimental data. All of our calculations have been carried out for identical ion-core scatterers at zero temperature.

Turning now to the experimental data of Porteus and Faith[22,23] on Al(111), we note that they find a large maximum near the energy of the kinematical primary Bragg peak in the (00) beam at $E = 51 \pm 1$ eV. Therefore, we concentrate on the primary beam energies near 50 eV for comparing the calculations with experiment in order to obtain numbers for the dispersion relation and damping of surface plasmons. Our analysis proceeds in three steps. First, for a given primary beam energy ($E = 50$ eV) and angle ($\theta = 15°$) the angular profiles (for fixed w) are analyzed to estimate C_2. Both initial and final azimuths are taken to be along the $\{110\}$ direction in the surface. At this stage of the calculation, we merely use reasonable numbers for the various surface-plasmon parameters, which can be obtained, for example, from Beck's RPA calculation.[8] The angular profile for $w = 14.4$ eV is the most influential in determining C_2. The second step is to choose a value of C_2 and calculate the loss profiles for various θ' as functions of $\hbar\omega_s$, C_1, and Γ_s. These calculations are repeated until the "best-fit" loss profile and the probable uncertainties in $\hbar\omega_s$, C_1, and Γ_s are determined. This analysis gives the best values of the parameters $\hbar\omega_s$, C_1, and Γ_s consistent with a particular value of C_2. Finally, the angular profiles are again calculated for the best dispersion relation and damping consistent with a given C_2, and are then compared with experiments. Bounds on the value of C_2 are obtained on the basis of a satisfactory description of the $w = 12.4$ and 14.4 eV angular profiles. The final selection of the optimum C_2 is made from a comparison of the angles of the predicted and observed subspecular ($\theta' < 15°$) maxima in the angular profiles.

The first step of the analysis leads to the range of values $6 \lesssim C_2 \lesssim 10$ eV Å^2. We show in Tables I–III the details of the second step where the best values of the coefficients in the dispersion relation and

TABLE I. Peaks in the loss profiles ($E = 50$ eV) obtained using the surface-plasmon dispersion relation $\hbar\omega_s(p_\parallel) = \hbar\omega_s + C_1 p_\parallel + 6p_\parallel^2$.

		w_{peak} (eV)					
			Theory				
θ' (deg)	$\hbar\omega_s$(eV)	Expt.	$C_1 = 4.0$	$C_1 = 2.5$	$C_1 = 1.0$	$C_1 = 0.5$	$C_1 = 0.25$
10		10.8	12.0	11.4	10.8	10.6	10.5
15	9.8	10.2	10.1	9.9	9.8	9.8	9.8
20		10.3	10.5	10.2	10.0	9.9	10.0
10		10.8	12.4	11.7	11.1	10.9	10.9
15	10.1	10.2	10.4	10.25	10.1	10.1	10.15
20		10.3	10.8	10.6	10.3	10.25	10.3
10		10.8	12.8	12.0	11.4	11.3	11.3
15	10.4	10.2	10.7	10.6	10.4	10.4	10.5
20		10.3	11.1	11.0	10.6	10.6	10.6

damping are found, for a given C_2, by comparing the location of the peaks in the experimental and the calculated loss profiles for three exit angles. As mentioned already, these calculations are done for $E = 50$ eV. If we accept the value of $C_2 = 10$ eV Å^2, then the best-fit parameters indicate a negative value of C_1. The dispersion relation and damping of surface plasmons are found to be

$$\hbar\omega_s(p_\parallel) = 10.1 - 0.7\,p_\parallel + 10\,p_\parallel^2 , \tag{21}$$

$$\Gamma_s(p_\parallel) = 0.9 + 0.74\,p_\parallel . \tag{22}$$

On the other hand, with the choice of $C_2 = 6$ eV Å^2, the best-fit parameters are

$$\hbar\omega_s(p_\parallel) = 10.1 + 0.5\,p_\parallel + 6\,p_\parallel^2 , \tag{23}$$

$$\Gamma_s(p_\parallel) = 0.8 + 0.74\,p_\parallel . \tag{24}$$

In all these formulas [Eqs. (21)–(24)], energy is measured in eV and $p_\parallel$ in Å^{-1}. In Fig. 1 we show a comparison of the calculated and measured loss profiles for three values of the exit angle. The calculated intensities associated with both dispersion relations [i.e., Eqs. (21)–(22) and (23)–(24)] are shown. The angular profiles also have been calculated for five loss energies w, with the two sets of dispersion and damping. They are compared with the experimental curves in Fig. 2. Table IV presents the angular location of the subspecular peaks in the two theories and the experiment. From Fig. 2 and Table IV, we see that the results obtained using the formulas of Eqs. (21) and (22) with $C_1 < 0$ seem preferable to those obtained using the other set.

Beck's RPA calculation[8] predicts $C_1 \cong 4$ eV Å, $C_2 \cong 3$ eV Å^2, $\Gamma_s \cong 0$, $D_1 \cong 0.1$ eV Å, and $D_2 \cong 0.1$ eV Å^2 for a background charge density comparable to that of aluminum. A detailed analysis of ILEED data on both Al(111) and Al(100) using these parameters may be found elsewhere.[35] Our present analysis indicates a serious deficiency in the existing microscopic-model calculations of the parameters characterizing surface plasmons. Equations (23)–(24) exhibit a positive C_1 which is in accord with most theoretical predictions. However, the coefficient of the quadratic term is unacceptably small, being responsible for the rapid movement of the surface-plasmon peak to smaller angles as w increases. The reason that we focus attention on the subspecular peak in the angular profile is that the superspecular peak often is absent in the experiments. This suggests that we should go beyond the kinematical two-step model in describing the elastic electron-solid scattering.

By using the above procedure we have tried to assess the uncertainty in the values of the various parameters which we derive from ILEED data. We assume in the theoretical calculation that $D_2 = 0$ and use D_1 mainly for fine corrections. Our method does not give a reliable estimate of D_1. The coefficient C_2 of the quadratic term can be estimated to an accuracy of about 20%. For the other surface-plasmon parameters, we think that the following ranges are representative: $\hbar\omega_s = 10.1 \pm 0.1$ eV, $C_1 = -0.7 \pm 0.3$ eV Å, and $\Gamma_s = 0.9 \pm 0.3$ eV. It is not surprising that RPA model calculations with an ideal

TABLE II. Peaks in the loss profiles ($E = 50$ eV) obtained using the surface-plasmon dispersion relation $\hbar\omega_s(p_\parallel) = \hbar\omega_s + C_1 p_\parallel + 8p_\parallel^2$.

			w_{peak} (eV)				
					Theory		
θ' (deg)	$\hbar\omega_s$(eV)	Expt.	$C_1 = 0.5$	$C_1 = 0.25$	$C_1 = 0.0$	$C_1 = -0.25$	$C_1 = -0.5$
10		10.8	11.1	11.0	10.9	10.8	10.7
15	9.8	10.2	9.9	9.85	9.8	9.8	9.8
20		10.3	10.15	10.1	10.0	10.0	10.0
10		10.8	11.4	11.3	11.2	11.1	11.0
15	10.1	10.2	10.2	10.2	10.2	10.2	10.1
20		10.3	10.4	10.4	10.35	10.2	10.2
10		10.8	11.75	11.6	11.5	11.4	11.35
15	10.4	10.2	10.5	10.45	10.4	10.4	10.4
20		10.3	10.7	10.6	10.6	10.6	10.3

TABLE III. Peaks in the loss profiles ($E = 50$ eV) obtained using the surface-plasmon dispersion relation $\hbar\omega_s(p_\parallel) = \hbar\omega_s + C_1 p_\parallel + 10 p_\parallel^2$.

θ' (deg)	$\hbar\omega_s$(eV)	w_{peak} (eV) Expt.	Theory $C_1 = 0.25$	$C_1 = 0.0$	$C_1 = -0.25$	$C_1 = -0.5$	$C_1 = -1.0$
10		10.8	11.6	11.5	11.4	11.3	11.1
15	10.1	10.2	10.2	10.2	10.15	10.1	10.05
20		10.3	10.4	10.4	10.4	10.3	10.2
10		10.8	12.0	11.8	11.8	11.6	11.4
15	10.4	10.2	10.5	10.4	10.45	10.4	10.4
20		10.3	10.7	10.7	10.6	10.6	10.6
10		10.8	12.3	12.2	12.1	12.0	11.8
15	10.7	10.2	10.8	10.8	10.8	10.7	10.7
20		10.3	11.0	11.0	10.95	10.85	10.8

surface show $\Gamma_s \equiv 0$. The fact that our analysis requires a finite Γ_s suggests the presence of imperfections at the surface, the importance of interband transitions, or both. Our value for Γ_s should be treated with some caution because it probably depends sensitively on the model for the electron-plasmon interaction vertex. An intrinsic limitation of our method of analysis is its lack of sensitivity to the behavior of the surface-plasmon dispersion relation for $p_\parallel \lesssim 0.2$ Å^{-1}. This means that we determine C_2 with greater confidence than the coefficient of the linear term C_1. We note that even though there is a substantial discrepancy between our value for C_1 and that calculated using the microscopic model, our result is not inconsistent with electron-transmission experiments on other materials.[10,17]

For the case in which the surface-plasmon dispersion relation and damping are given by Eqs. (21) and (22), we have compared our model predictions with the experimental data for incident electron energies away from the energy of the peak in the elastic intensity. Figures 3 and 4 illustrate the comparison of the experimental loss and angular profiles with the theoretical curves for $E = 60$ eV, where processes involving (surface-plasmon) loss before diffraction should dominate diffraction-before-loss processes. The s-wave model is less accurate in this region of energies. As Figs. 3 and 4 demonstrate, the agreement between theory and experiment is still reasonable at $E = 60$ eV, although it is perhaps less satisfactory than at $E = 50$ eV. Finally, Fig. 5 illustrates the comparison of calculated and experimental angular profiles for a number of primary beam energies E and a fixed loss energy $w = 14.4$ eV.

We turn next to our analysis of the experimental results of Burkstrand and Propst,[24] who have studied the (10) and (11) diffracted beams of electrons incident normally on an Al(100) surface. Their results often are quite complex, especially for low incident energies, with multiple scattering effects obscuring the predictions of a simple two-step kinematical model. Consequently, we have not tried to derive parameters for the surface-plasmon dispersion and damping from these experiments. Rather, we attempted to isolate interesting qualitative features of the data which can be interpreted by the two-step model. In comparing the model predictions with the experimental data, we have used the best-fit surface-plasmon parameters obtained from an analysis of Porteus's experiments, viz., Eqs. (21) and (22). We discuss below two interesting complexities evident in the data which admit an elementary interpretation in terms of the two-step model.

In Burkstrand's experiments on the loss profiles for the (11) beam, the relative heights of the

TABLE IV. Peaks in the angular profile for $\theta' < 15°$.

w (eV)	θ_{peak} (deg) Expt.	Theory $\hbar\omega_s(p_\parallel) = 10.1 + 0.5 p_\parallel + 6 p_\parallel^2$	$\hbar\omega_s(p_\parallel) = 10.1 - 0.5 p_\parallel + 8 p_\parallel^2$	$\hbar\omega_s(p_\parallel) = 10.1 - 0.7 p_\parallel + 10 p_\parallel^2$
8.4	11	12.25	12.4	13
10.4	12.5	12.8	12.4	13
12.4	8.25	6.8	7	7.9
14.4	5	2.7	3.5	4.75
16.4	7.25	•••	0.5	2

surface- and bulk-plasmon peaks vary with both the primary electron energy and the angle of observation.

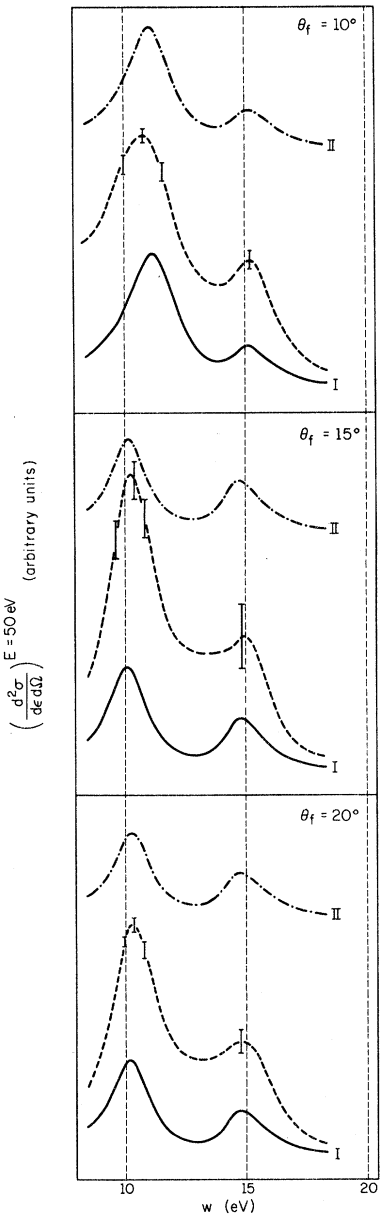

FIG. 1. Comparison of the experimental (dashed lines) and two sets of theoretical (marked I and II) loss profiles for the (00) beam of electrons on Al(111). The primary beam energy is 50 eV, the angle of incidence is 15°, the exit angles are noted by θ_f, and both initial and final beam lie along a {110} direction in the surface plane. Elastic electron–ion-core scattering is described by the s-wave inelastic-collision model with $\lambda_{ee}=6$ Å, $V_0=14.7$ eV, and $\delta=\frac{1}{4}\pi$. Curve I refers to calculations performed using the surface-plasmon dispersion relation and damping of $\hbar\omega_s(p_\parallel)=10.1-0.7p_\parallel+10p_\parallel^2$, $\Gamma_s(p_\parallel)=0.9+0.74p_\parallel$. Curve II refers to $\hbar\omega_s(p_\parallel)=10.1+0.5p_\parallel+6p_\parallel^2$, $\Gamma_s(p_\parallel)=0.8+0.74p_\parallel$. The error bars on the experimental curves indicate typical uncertainties. The dashed line is a computer-averaged value.

tion. This effect is induced by the elastic electron-solid diffraction, and its qualitative features are successfully reproduced by our model. Figure 6 shows theoretical and experimental loss profiles for the (11) beam for three primary energies and three exit angles. The experimental data are taken in the direction of elastic diffraction θ_E, and at $2\frac{1}{2}°$ on either side of this direction. Theoretical curves have been computed for exit angles of $\theta_E-1\frac{1}{2}°$, $\theta_E+1°$, and $\theta_E+3\frac{1}{2}°$ because the particular loss-profile characteristics are best displayed theoretically for angles shifted through 1° relative to the experimental angles (which are themselves uncertain to within this amount). As indicated in the figure, the bulk-plasmon peak is higher than the surface-plasmon peak for larger angles of emergence and greater electron incident beam energies. This effect is observed in both the experimental and the theoretical curves, even though they do not agree too well in detail. Thus the apparently complicated dependence of the loss profiles on the beam parameters is an immediate consequence of two-step inelastic diffraction.

A second interesting aspect of inelastic diffraction involving bulk plasmons is the phenomenon of "sideband diffraction,"[19,36] whereby the single bulk-plasmon peak in the angular profile is split into two. This is caused by vestiges of momentum conservation in the direction normal to the metal surface. If, simultaneously with Eq. (17), the electron momenta satisfy the condition (for an fcc crystal)

$$\mathrm{Re}[k'_\perp(0, E-w)+k_\perp(0, E)]=\pm p_\perp+(2n+1)\pi/d\,, \quad (25)$$

where d is the spacing between atomic layers and $p_\perp$ is determined from

$$w=\hbar\omega_b(\vec{p}_\parallel, p_\perp)\,, \quad (26)$$

then the bulk-plasmon peak in the angular profile may be split into two peaks. Sideband diffraction is displayed clearly in Fig. 7, which shows a comparison of the theoretical and experimental angular profiles for the (11) beam for a number of primary electron energies. The loss energy is fixed at 16 eV. The peak on the left in the theoretical curves is caused by surface plasmon. As the primary beam energy is increased, one of the sideband peaks gains in intensity relative to the other, and this shows up in the movement of the bulk-plasmon peak across the direction of elastic diffraction which is denoted in the figure by dots. It seems appropriate to emphasize the facts that the two-step model enables us to understand the origin of the prominent structures in the experimental data even though it cannot explain the data in detail, and that the absolute values of the experimental collector angles exhibit a large (±4°) uncertainty.

In Fig. 8 we show theoretical and experimental angular profiles for the (11) beam for a number of

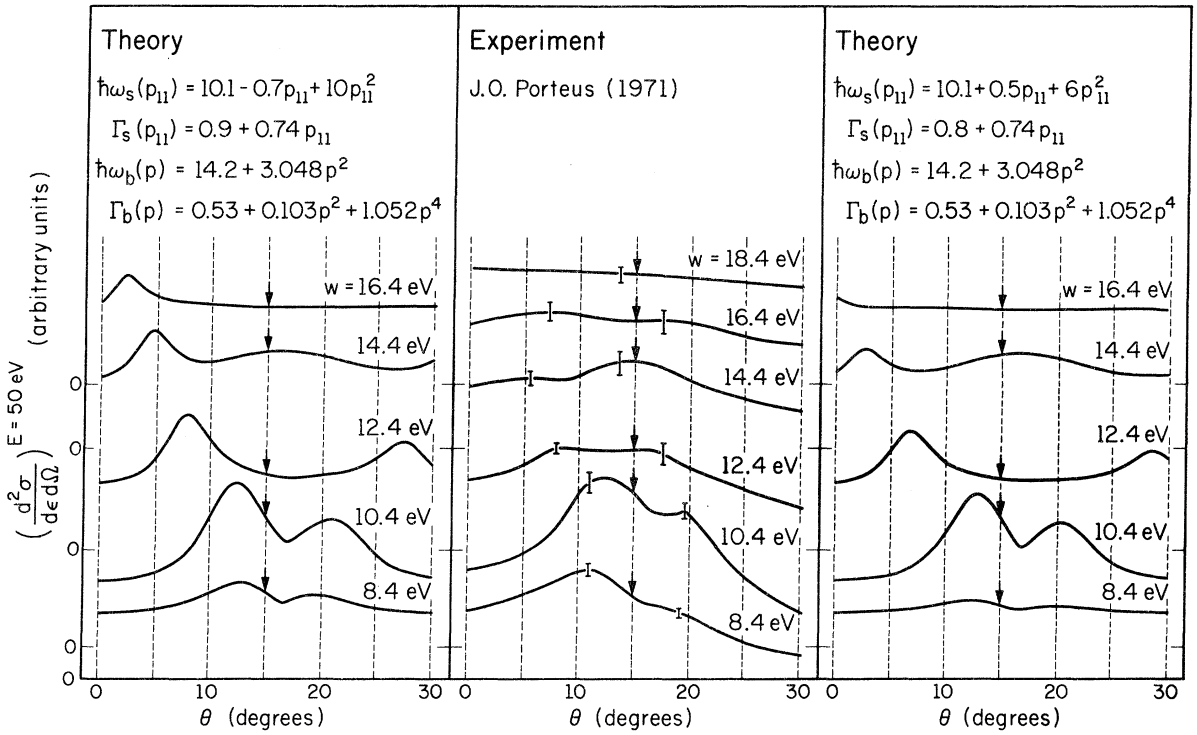

FIG. 2. Theoretical and computer-averaged experimental angular profiles for electrons incident on Al(111) with a primary energy E of 50 eV and diffracted inelastically in the (00) direction for a number of loss energies w. Arrows indicate the direction of specular reflection ($\theta_i = 15°$) and bars typical experimental uncertainties. Two sets of theoretical curves are given with their dispersion relations noted in the figure. The parameters used to describe the elastic scattering are specified in the caption to Fig. 1.

loss energies w, when the incident electron has the energy of a primary Bragg peak ($E_B = 86$ eV). Processes involving diffraction before loss dominate the scattering cross section at this energy. The theory is qualitatively successful in describing the variation of the intensity of scattered electrons as a function of the energy loss. It also can explain the observed structures in the experimental curves at $w = 12$–16 eV. The theory is perhaps less successful describing the experimental data for the incident electron energy of 96 eV when loss-before-diffraction processes are predominant. The theory and the experiment at this energy are compared in Fig. 9. The qualitative features of the data are described adequately for $10 \leq w \leq 14$ eV.

We have analyzed Burkstrand's experimental ILEED data for the (10) diffracted beam from an Al(100) surface in the same way as for the (11) beam. Again we find general agreement between theory and experiment, although in detail the agreement is poor. In Fig. 10 we show a comparison of the theoretical and experimental angular profiles for the (10) beam for a number of incident energies of the electron when the loss energy is kept fixed at $w = 16$ eV. Finally, we recall that although the curves shown in the figures have been calculated with an s-wave model for the electron–ion-core scattering, we have carried out calculations with a more exact, angle-dependent APW scattering cross section[37,38] and found no significant change in the theoretical predictions.

IV. SUMMARY AND CONCLUSIONS

The main result of the analysis that we have presented in this paper is that inelastic low-energy-electron diffraction may be used to determine, quantitatively, plasmon dispersion relations which characterize the electronic structure of a surface. That is, we argue that the two-step model describes the basic processes of ILEED sufficiently well that we may use it to analyze ILEED data for extracting quantitative information about the elementary excitation spectra of simple metals. We have substantiated this claim by describing the application of the two-step model of inelastic diffraction to determine the surface-plasmon dispersion relation and damping on Al(111) for $10^{-2} \lesssim p_{\parallel} \lesssim 1$ Å^{-1}. The use of the microscopic two-step model (as opposed to semiclassical "single-step" models[21]) is essential to the analysis in order to identify the dynamical origin of the various resonant peaks in the loss and angular profiles. A significant aspect of Eqs. (16) and (20)

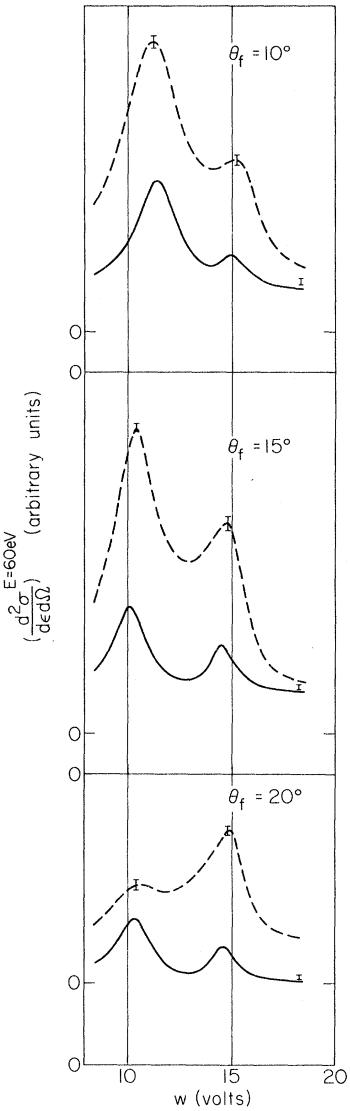

FIG. 3. Comparison of the computer-averaged experimental (dashed lines) and the theoretical (solid lines) loss profiles for the (00) beam of electrons incident at an angle of 15° on Al(111) with a primary energy E of 60 eV. Bars denote typical experimental uncertainties and θ_f the exit angles. The parameters for elastic scattering are the same as in Fig. 1. The theoretical curves have been calculated for the surface-plasmon dispersion and damping given by Eqs. (21) and (22) of the text.

is that the inelastic scattering cross section has the form of a vertex function of p multiplied by a plasmon spectral density, $\mathrm{Im}D(\vec{p}, w) = \Gamma\{[w - \hbar\omega(\vec{p})]^2 + \Gamma^2\}^{-1}$. As a result, features of the model predictions which depend primarily on the behavior of these features are insensitive to the detailed model of the elastic electron-solid scattering. Such a feature is the location of the maxima in $(d^2\sigma/d\epsilon d\Omega)_{sp}$ for fixed E, θ, ψ, and ψ' and $w > \hbar\omega_s$ as a function

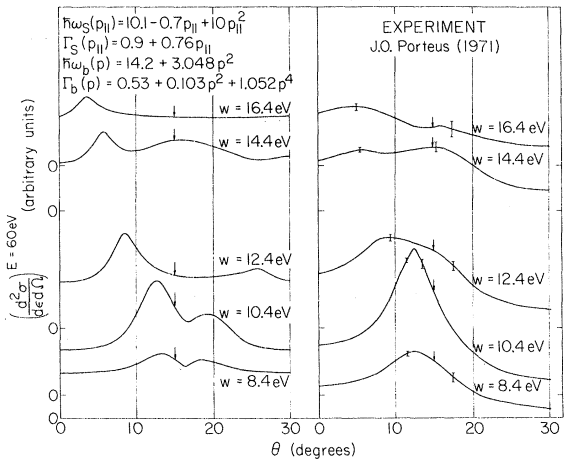

FIG. 4. Theoretical and computer-averaged experimental angular profiles for the inelastically diffracted (00) beam of electrons incident at an angle of 15° on Al(111) with a primary beam energy of 60 eV. Arrows denote the specular direction, bars typical experimental uncertainties, and w the loss energies. Elastic scattering is described by the same parameters as in Fig. 1. The plasmon-dispersion relation and damping that are used in the model calculation are noted in the figure and in Eqs. (21) and (22) in the text.

of θ' [i.e., $p_{||}$ via Eq. (17)]. The location of these maxima as a function of (θ', w) for fixed values of E, θ, $\psi = \psi' + \pi$ is a direct reflection of the surface-plasmon dispersion relation of Eq. (1), independent of other aspects of the model. Therefore our meth-

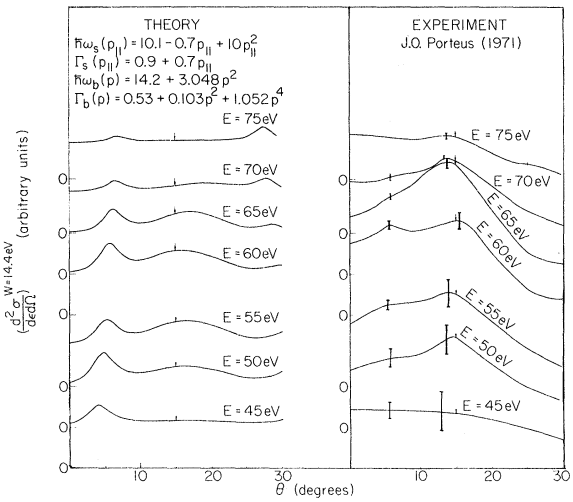

FIG. 5. Theoretical and computer-averaged experimental angular profiles for the inelastically diffracted (00) beams of electrons incident on Al(111) for a number of primary energies E and a fixed loss energy of $w = 14.4$ eV. Arrows indicate the direction of specular reflection ($\theta_i = 15°$) and bars typical experimental uncertainties. The parameters used in the model calculation are given by Eqs. (21) and (22) in the text.

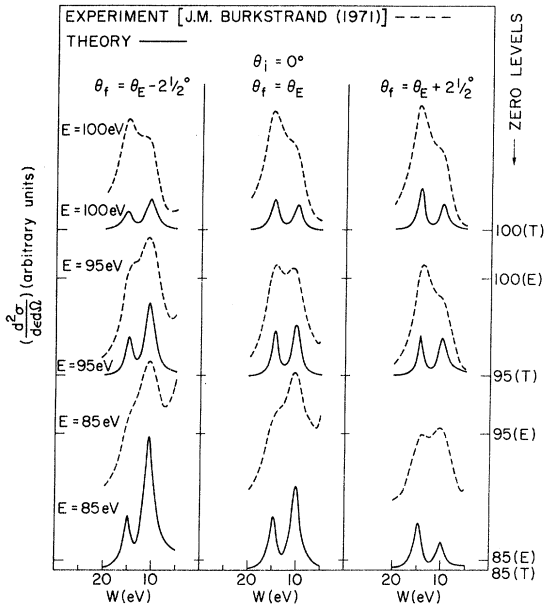

FIG. 6. Comparison of theoretical (full lines) and experimental (dashed lines) loss profiles of electrons incident normally on Al(100) and scattered inelastically in the (11) beam. The primary beam energy is denoted by E, which also labels the zero levels on the right-hand side of the graph. The notation $T(E)$ designates the theoretical (experimental) curve. The exit angles in the experiment are denoted by θ_f, while θ_E defines the direction of the elastically diffracted beam. The theoretical curves in each vertical panel are computed for an emergence angle 1° above the measured exit angle (see text; the absolute value of this angle may be in error by as much as ± 4°). The parameters for the surface-plasmon dispersion and damping used in the theory are given in Eqs. (21) and (22) of the text. Elastic electron–ion-core scattering is described by the s-wave inelastic-collision model with $\lambda_{ee} = 8$ Å, $V_0 = 16.7$ eV, and $\delta = \frac{1}{4}\pi$. For these parameters, the kinematically calculated (11) beam intensities exhibit a primary Bragg peak at $E_B = 86$ eV. A large peak occurs in the experimental (11) intensity profile at this energy.

od of analysis should give reliable values of the parameters in the dispersion relation of surface plasmons. The damping, however, is determined much less accurately because it depends on the exact form of the electron–surface-plasmon vertex function, which is poorly known.

Two "technical" limitations of our analysis are the use of an s-wave model for the electron–ion-core scattering and that of the first Born approximation (kinematical model) to describe the elastic scattering of electrons by the lattice. Although the s-wave model gives a poor description of electronic scattering by aluminum ions, as noted in Sec. III we found that within our two-step model the predictions of the theory were not significantly modified when the angular dependence of the electron–ion-core scattering was included in the calculation. Therefore, the s-wave model appears quite acceptable, although the consequences of the kinematical approximation probably are more serious. In this paper we have described the elastic electron-lattice scattering simply by the ion-core scattering amplitude $t(E)$. A complete calculation of the single-plasmon-emission cross sections requires that we evaluate the elastic scattering amplitudes T_ν of the electrons from the νth atomic layer by an appropriate matrix-inversion method and use these T_ν to compute the inelastic intensities.[39] Such an inclusion of multiple scattering may depress the superspecular peak due to surface plasmons and make the theoretical angular profiles agree more closely with the existing experimental data.

Another problem with our version of the theory is that it does not take into account properly the electron-solid force law when the electron is outside the metal. At long distances from the surface the electron moves "as if" it were affected by the familiar image potential, although in fact it is under the influence of a nonlocal potential.[3] The nonlocality of the potential comes principally from the lack of translational invariance in the direction normal to the metal surface. The electron-solid potential has been calculated[3] in the random-phase approximation for certain models of the half-space electron gas. Any precise theory of both elastic and inelastic LEED must start with electron waves distorted by this nonlocal optical potential prior to the electron's scattering by the short-range ion-core potentials. Work is now in progress incorporating this aspect of the electron-solid force law into the theory.

In spite of its limitations, we believe that our semiphenomenological model of two-step inelastic diffraction gives reliable numbers for the dispersion relation of surface plasmons on Al(111). Our analysis leads us to conclude that microscopic models[8,9] for studying the surface-plasmon dispersion are seriously in error. A similar conclusion had been reached previously[17] on the basis of a hydrodynamic-model analysis of keV electron scattering data for Mg.[10] This suggests that the form of the electron-density profile near a surface may have a more profound influence on the dispersion of surface plasmons than has been realized so far.

Note Added in Proof. The original computer program used to construct the figures and dispersion relations Eqs. (21)–(24) contained an error in that the bulk-plasmon contributions to the intensity were too large by a factor of 2. Line shapes comparable to those shown in the figures are obtained from the corrected program by increasing Γ_s [see Eq. (2)] by about 70%. Therefore Eqs. (22) and (24) become

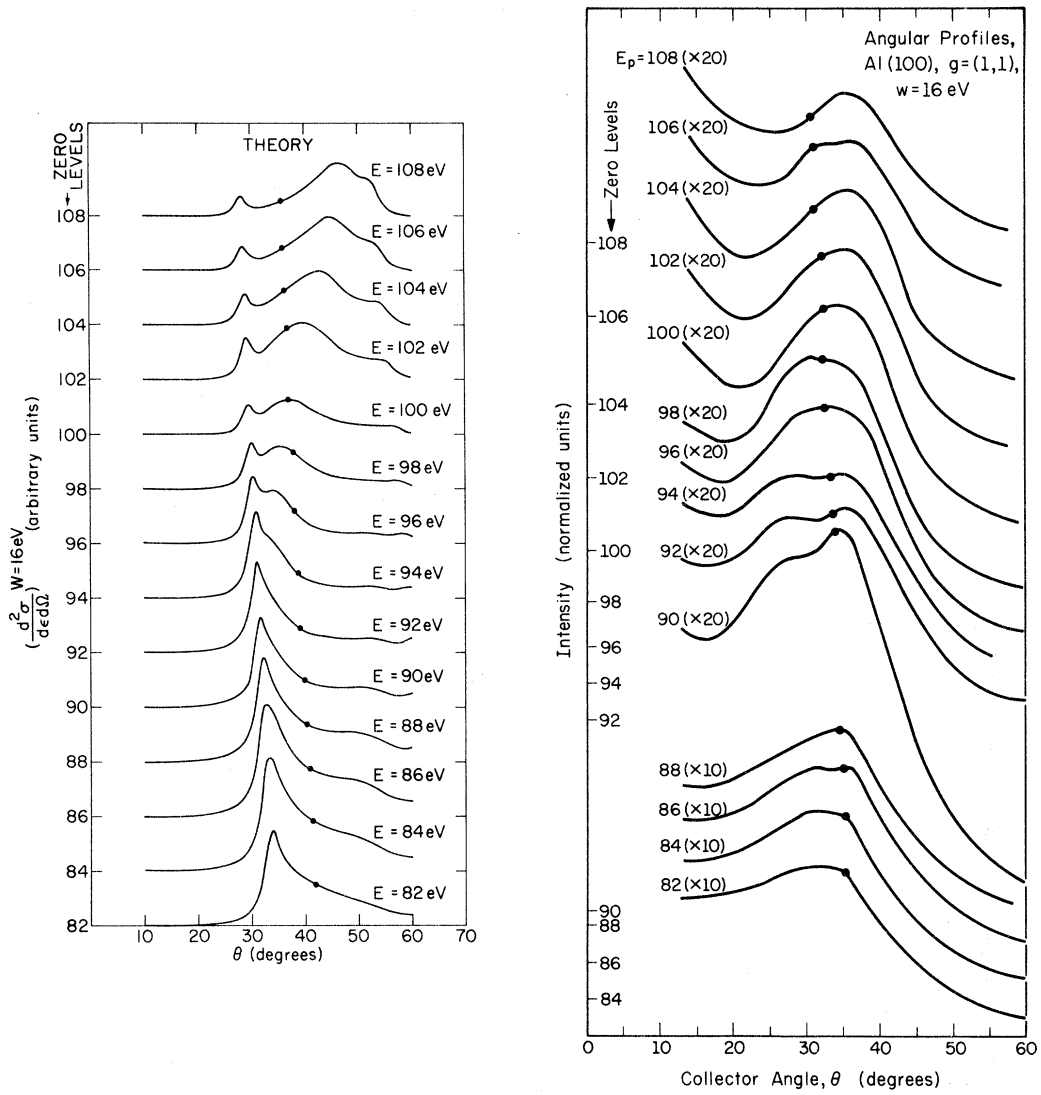

FIG. 7. Theoretical and experimental curves for the angular profile of electrons incident normally on Al(100) and scattered inelastically in the (11) beam. The loss energy is fixed at 16 eV and the primary beam energy E is varied. Dots indicate the direction of emergence of the elastically scattered (11) beam. All parameters that are used in the model calculations are indicated in the caption to Fig. 6. The experimental collector angle is uncertain to within ± 4° because of uncertainties in target and beam alignment and the angular spread of the incident beam.

$$\Gamma_s(P_{\parallel}) = 1.6 + 0.74\ P_{\parallel}\,, \tag{22a}$$

$$\Gamma_s(P_{\parallel}) = 1.5 + 0.74\ P_{\parallel}\,, \tag{24a}$$

respectively. The range of values for Γ_s is $\Gamma_s = 1.5 \pm 0.3$ eV. Other parameters in the dispersion relations are unchanged.

ACKNOWLEDGMENTS

The authors wish to thank Dr. G. E. Laramore and Dr. P. J. Feibelman for many valuable discussions of the model. They are also indebted to Dr. J. O. Porteus, Professor F. M. Propst, and J. M. Burkstrand for copies of their unpublished data and for permission to reproduce them here.

APPENDIX

In this appendix we derive an expression [cf. Eq. (16)] for the inelastic scattering cross section of an electron exciting a surface plasmon in the two-step inelastic diffraction model. The starting formula is Eqs. (4.14) in the first of Refs. 18, which can be written for the case of surface plasmons as

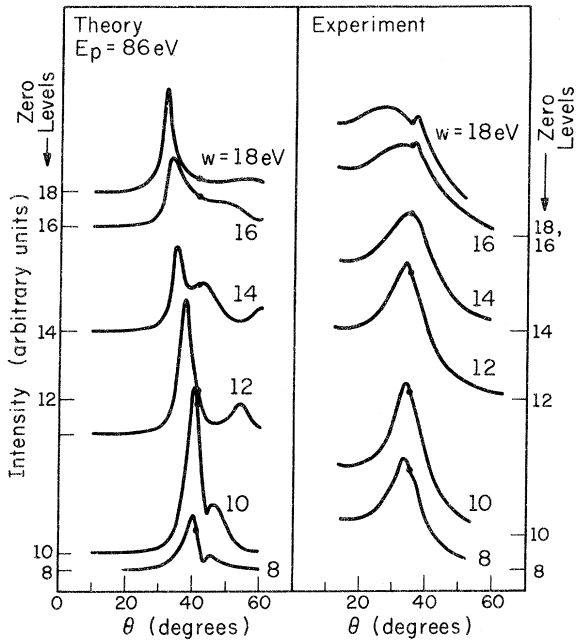

FIG. 8. Theoretical and experimental angular profiles for electrons incident normally on Al(100) with a primary energy of 86 eV and diffracted elastically in the (11) direction. The loss energy w is varied. Dots denote the direction of emergence of the elastically diffracted beam. Elastic scattering parameters and the surface-plasmon dispersion and damping that are used in the theory are the same as for Fig. 6. The experimental exit angle is uncertain to within ± 4° because of uncertainties in target and beam alignment and the angular spread of the incident beam.

$$\left(\frac{d^2\sigma}{d\epsilon\, d\Omega}\right)^{(4)}_{sp} = \left(\frac{E-w}{E}\right)^{1/2} \frac{1}{2\pi} \int \frac{d^2p_{\parallel}}{(2\pi)^2} \left[-2N(-w)\,\mathrm{Im}D_s(\vec{p}_{\parallel}, w)\right] \times\left[\left|A_{2b}(\vec{k}', \vec{k}, \vec{p}_{\parallel}, E) + A_{2c}(\vec{k}', \vec{k}, \vec{p}_{\parallel}, E-w)\right|^2\right], \tag{A1}$$

$$A_{2b}(\vec{k}', \vec{k}, \vec{p}_{\parallel}, E) = \int \frac{d^3k_1}{(2\pi)^3} A(\vec{k}', \vec{k}_1, \vec{p}_{\parallel})\, G(\vec{k}_1, E)\, T_1(\vec{k}_1, \vec{k}, E), \tag{A2}$$

$$A_{2c}(\vec{k}', \vec{k}, \vec{p}_{\parallel}, E-w) = \int \frac{d^3k_1}{(2\pi)^3} T_1(\vec{k}', \vec{k}_1, E-w)\, G(\vec{k}_1, E-w) \times A(\vec{k}_1, \vec{k}, \vec{p}_{\parallel}), \tag{A3}$$

$$T_1(\vec{k}', \vec{k}, E) = \sum_m t(E)\, e^{-i(\vec{k}'-\vec{k})\cdot\vec{R}_m}, \tag{A4}$$

$$A(\vec{k}', \vec{k}, \vec{p}_{\parallel}) = \frac{2\pi m}{h^2} \sum_n \left(\frac{\pi e^2\hbar\omega_s}{p_{\parallel}}\,\Omega^2\right)^{1/2} e^{-i(\vec{k}'-\vec{k}-\vec{p}_{\parallel})\cdot\vec{R}_n} \times e^{-p_{\parallel}|R_{n\perp}|}. \tag{A5}$$

The quantities $N(w)$ and $D_s(\vec{p}_{\parallel}, w)$ are given by Eqs. (5) and (7), respectively, while the electron–ion-core scattering amplitude $t(E)$ is given by Eq. (3). $G(\vec{k}_1, E)$ denotes the electron propagator in the intermediate state. It is straightforward to carry out the sum over atomic sites parallel to the surface and the integral over the intermediate momentum variable k_1. We obtain

$$A_{2b}(\vec{k}', \vec{k}, \vec{p}_{\parallel}, E) = \frac{2\pi m t(E)}{h^2} \left(\frac{\pi e^2\hbar\omega_s}{p_{\parallel}}\,\Omega^2\right)^{1/2} \frac{2\pi^2}{A^2} \times\sum_{\vec{g}} \delta(\vec{k}'_{\parallel} - \vec{k}_{\parallel} - \vec{p}_{\parallel} - \vec{g}) \left(-\frac{im}{\hbar^2 k_{\perp}(\vec{g}, E)}\right) S_b(\vec{g}, E), \tag{A6}$$

where A is the area of the unit cell whose volume is Ω, and $S_b(\vec{g}, E)$ is defined as

$$S_b(\vec{g}, E) = \sum_{\nu=-\infty}^{\infty} \sum_{\mu=0}^{\infty} e^{ik'_{\perp}d\nu}\, e^{-p_{\parallel}d|\nu|}\, e^{i(k_{\perp}d - \vec{g}\cdot\vec{a})\mu} \times e^{ik_{\perp}(\vec{g}, E)|\nu-\mu|d}. \tag{A7}$$

We have introduced here the convention of Duke and

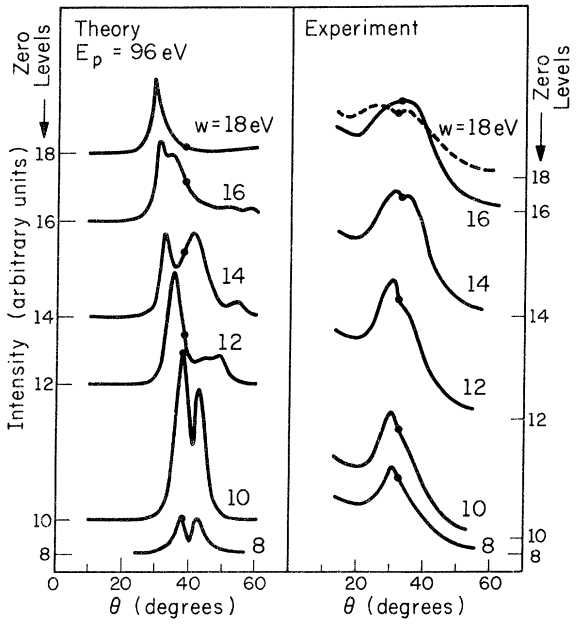

FIG. 9. Theoretical and experimental angular profiles for the inelastically diffracted (11) beam of electrons incident normally on Al(100) with a primary energy E of 96 eV. The loss energy w is the variable and dots indicate the direction of the elastically diffracted (11) beam. Elastic scattering parameters and the damping and dispersion relation of surface plasmons entering the theory are the same as for Fig. 6. The experimental exit angle is uncertain to within ± 4° because of uncertainties in the target and beam alignment and the angular spread of the incident beam.

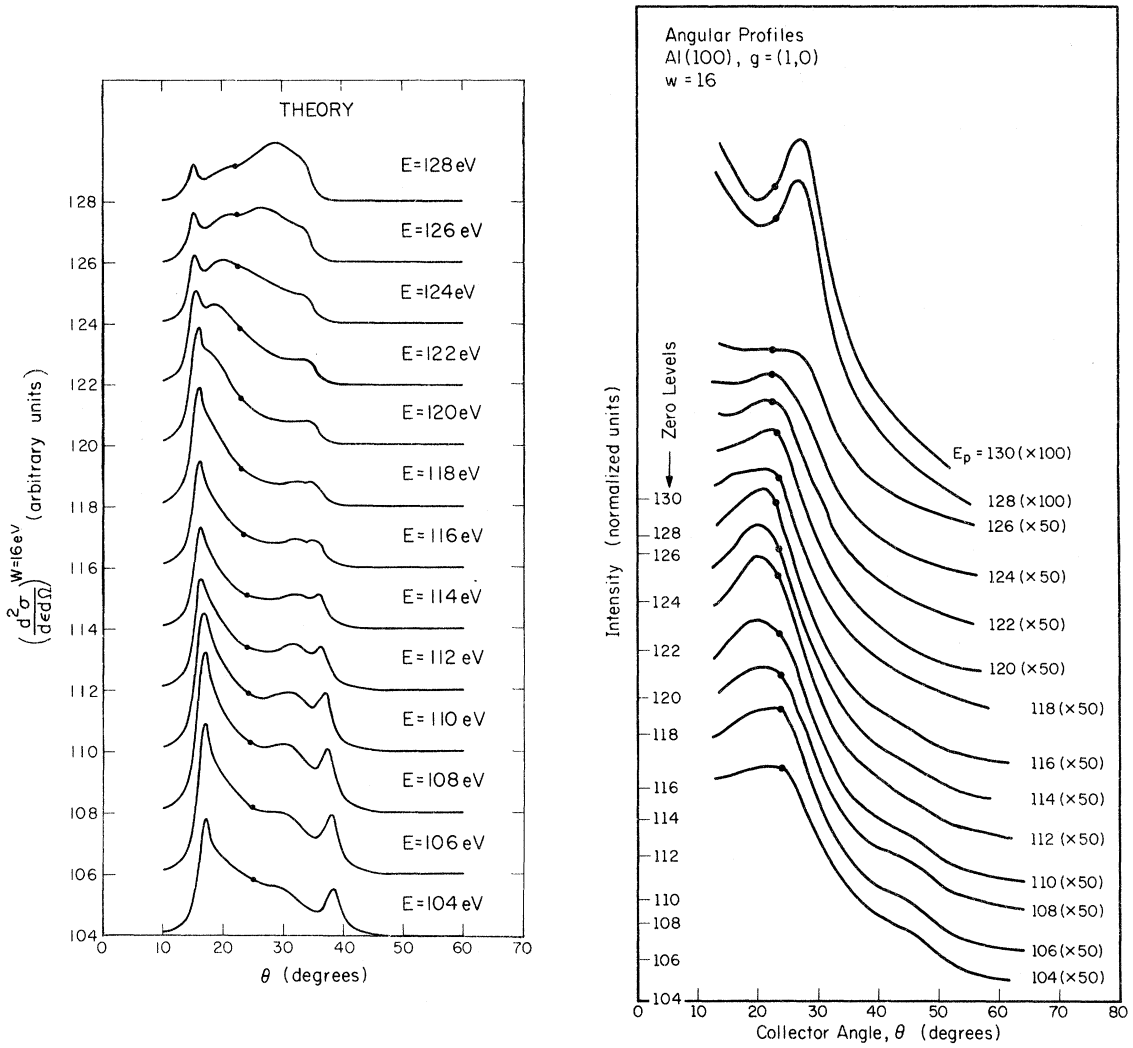

FIG. 10. Comparison of the theoretical and experimental angular profiles of electrons, incident normally on Al(100), which are scattered inelastically in the (10) direction. The primary beam energy E is varied while the loss energy w is fixed at 16 eV. The direction of the elastically diffracted (10) beam is specified by dots. The parameters of the surface-plasmon dispersion and damping used in the theory are given in Eqs. (21) and (22) of the text. Elastic electron-ion scattering is described by the model of s-wave scatterers with $\lambda_{ee}=8$ Å, $V_0=14$ eV, and $\delta=\frac{1}{4}\pi$. The experimental collector angle is uncertain to within ± 4° because of uncertainties in target and beam alignment and the angular spread in the incident beam. The experimentally measured elastic intensity profiles and the kinematically calculated theoretical intensity profiles both exhibit a "primary Bragg" peak at $E=108$ eV.

Laramore[18] of measuring the normal momentum of the scattered electron as positive for backscattering. The normal component of the electron momentum in the intermediate state is denoted by $k_\perp(\vec{g}, E)$, which is given by Eq. (14) when the electron is inside the metal. When the electron is outside the metal, the normal momentum is $\tilde{k}_\perp(\vec{g}, E)$ defined as in Eq. (14) with $\Sigma(E)$ set equal to zero. We obtain for the amplitude of the process of loss before diffraction

$$A_{2c}(\vec{k}'_{\parallel}, \vec{k}, \vec{p}_{\parallel}, E-w)=\frac{2\pi mt(E-w)}{\hbar^2}\left(\frac{\pi e^2\hbar\omega_s}{p_{\parallel}}\Omega^2\right)^{1/2}$$

$$\times\frac{(2\pi)^2}{A^2}\sum_{\vec{g}}\delta(\vec{k}'_{\parallel}-\vec{k}_{\parallel}-\vec{p}_{\parallel}-\vec{g})\left(\frac{-im}{\hbar^2 k'_\perp(-g, E-w)}\right)$$

$$\times S_c(\vec{g}, E)\,, \qquad \text{(A8)}$$

where

$$S_c(\vec{g}, E)=\sum_{\nu=-\infty}^{\infty}\sum_{\mu=0}^{\infty} e^{ik_\perp d\nu}\, e^{-p_{\parallel}d|\nu|}\, e^{i(k'_\perp d-\vec{g}\cdot\vec{a})\mu}$$

$$\times e^{ik'_\perp(-\vec{g}, E-w)d|\mu-\nu|}\,. \qquad \text{(A9)}$$

The sums in Eqs. (A7) and (A9) can be evaluated easily. Note that $S_c(\vec{g}, E)$ can be obtained from $S_b(\vec{g}, E)$ by interchanging $k_\perp$ and $k'_\perp$ and redefining the

momentum variable in the intermediate state. Therefore we consider only $S_b(\vec{g}, E)$ (i.e., loss before diffraction). The sums in Eq. (A7) may be decomposed into three distinct contributions. When $\nu < 0$ and $\mu > 0$, the contribution comes from electrons outside the metal interacting with surface plasmons. For $\mu > \nu > 0$ we have the situation when the energy-loss process occurs closer to the metal surface than elastic diffraction. This is the contribution retained by Duke and Laramore.[18] Finally, $\nu > \mu > 0$ describes the situation when the loss process occurs deeper into the metal than elastic diffraction. We evaluated the amplitude for this last process and found it to be small compared to the other two. In what follows we neglect this contribution. We can then write

$$S_b(\vec{g}, E) = S_b^{(1)}(\vec{g}, E) + S_b^{(2)}(\vec{g}, E) , \tag{A10}$$

where $S_b^{(1)}(\vec{g}, E)$ is the part coming from losses occurring outside the solid and $S_b^{(2)}(\vec{g}, E)$ comes from losses occurring inside. In the jellium model, the surface-plasmon field is continuous rather than cell periodic, so that the sum over ν in Eqs. (A7) and (A9) should be converted to an integral.[18] Accordingly, we find

$$S_b^{(1)}(\vec{g}, E) = \int_{-\infty}^{0} d\nu \sum_{\mu=0}^{\infty} e^{i\vec{k}_\perp' d\nu} e^{p_\parallel d\nu} e^{i(k_\perp d - \vec{g}\cdot\vec{a})\mu} \times e^{ik_\perp(\vec{g},E)d\mu} e^{-i\vec{k}_\perp(\vec{g},E)d\nu}$$

$$= (1 - e^{i\{[k_\perp + k_\perp(\vec{g},E)]d - \vec{g}\cdot\vec{a}\}})^{-1} \times \frac{1}{p_\parallel d + i[\vec{k}_\perp' - \vec{k}_\perp(\vec{g}, E)]\, d} . \tag{A11}$$

For evaluating $S_b^{(2)}(\vec{g}, E)$ we may ignore the "central-cell" corrections discussed in Refs. 18 because the inelastic scattering vertex describes forward scattering. This point has been discussed in detail by Laramore and Duke,[18] who find that

$$S_b^{(2)}(\vec{g}, E) = \sum_{\nu=0}^{\infty} \sum_{\mu=\nu}^{\infty} e^{ik_\perp' d\nu} e^{-p_\parallel d\nu} e^{i(k_\perp d - \vec{g}\cdot\vec{a})\mu} \times e^{ik_\perp(\vec{g},E)d\mu} e^{-ik_\perp(\vec{g},E)d\nu}$$

$$= \frac{1}{1 - e^{i[k_\perp d + k_\perp(\vec{g},E)d - \vec{g}\cdot\vec{a}]}} \times \frac{1}{1 - e^{i(k_\perp + k_\perp')d - p_\parallel d - i\vec{g}\cdot\vec{a}}} . \tag{A12}$$

When Eq. (A6) is combined with Eqs. (A10)–(A12), we arrive at $A_b'(\vec{g}, E)$ of Eq. (18). $A_c'(\vec{g}, E - w)$ of Eq. (19) is derived similarly. Equation (16) for the scattering cross section is obtained trivially if we assume that $w \gg \kappa T$ and take

$$\mathrm{Im} D_s(\vec{p}_\parallel, w) = \Gamma_s(p_\parallel) / \{[w - \hbar\omega_s(p_\parallel)]^2 + [\Gamma_s(p_\parallel)]^2\} .$$

*Work supported in part by the Advanced Research Projects Agency under Contract No. HC 15-67-C-0221, by the U.S. Air Force Office of Scientific Research, Office of Aerospace Research, under Grant No. AFOSR-71-2034, and by the Joint Services Electronics Program under Contract No. DAAB-07-67-C-0199.

[1]R. H. Ritchie, Phys. Rev. 106, 874 (1957).
[2]E. A. Stern and R. A. Ferrell, Phys. Rev. 120, 130 (1960).
[3]P. J. Feibelman, C. B. Duke, and A. Bagchi (unpublished).
[4]H. Kanazawa, Progr. Theoret. Phys. (Kyoto) 26, 851 (1961).
[5]R. H. Ritchie and A. L. Marusak, Surface Sci. 4, 234 (1966).
[6]P. A. Fedders, Phys. Rev. 153, 438 (1967).
[7]P. J. Feibelman, Phys. Rev. 176, 551 (1968).
[8]D. E. Beck, Phys. Rev. B 4, 1555 (1971).
[9]Ch. Heger and D. Wagner, Phys. Letters 34A, 448 (1971); Z. Physik 244, 449 (1971).
[10]A. J. Bennett, Phys. Rev. B 1, 203 (1970).
[11]C. J. Powell and J. B. Swan, Phys. Rev. 115, 869 (1959).
[12]C. J. Powell and J. B. Swan, Phys. Rev. 116, 81 (1959).
[13]H. Raether, Colloque J. Phys. 31, 59 (1970).
[14]Y. Y. Tong and E. A. Stern, Phys. Rev. Letters 19, 511 (1967).
[15]N. Marshall, B. Fischer, and H. J. Queisser, Phys. Rev. Letters 27, 95 (1971).
[16]J. Thirlwell, Proc. Phys. Soc. (London) 91, 552 (1967).
[17]C. Kunz, Z. Physik 196, 311 (1966).
[18]C. B. Duke and G. E. Laramore, Phys. Rev. B 3, 3183 (1971); 3, 3198 (1971).
[19]C. B. Duke, G. E. Laramore, and V. Metze, Solid State Commun. 8, 1189 (1970).
[20]K. L. Ngai, E. N. Economou, and M. H. Cohen, Phys. Rev. Letters 24, 61 (1970).
[21]A. A. Lucas and M. Sunjić, Phys. Rev. Letters 26, 229 (1971).
[22]J. O. Porteus and W. N. Faith, in Proceedings of the Fifth Low-Energy Electron Diffraction Seminar [Natl. Bur. Std. (U.S.) Lecture Notes, Washington, D.C., 1971], pp. 81–85 (unpublished).
[23]J. O. Porteus (unpublished).
[24]J. M. Burkstrand and F. M. Propst, J. Vac. Sci. Technol. (to be published).
[25]J. C. Turnbull and H. E. Farnsworth, Phys. Rev. 54, 507 (1938).
[26]P. P. Reichertz and H. E. Farnsworth, Phys. Rev. 75, 1902 (1949).
[27]C. B. Duke and C. W. Tucker, Jr., Surface Sci. 15, 231 (1969).
[28]C. B. Duke and C. W. Tucker, Jr., Phys. Rev. Letters 23, 1163 (1969).
[29]J. I. Gersten, Phys. Rev. 188, 774 (1969).
[30]C. von Festenberg, Phys. Letters 23, 293 (1966).
[31]A. Bagchi, C. B. Duke, P. J. Feibelman, and J. O. Porteus, Phys. Rev. Letters 27, 998 (1971).
[32]P. Schmüser, Z. Physik 180, 105 (1964).
[33]J. Geiger and K. Wittmaack, Z. Physik 195, 44 (1966).
[34]C. Kunz, Z. Physik 167, 53 (1962).

[35]C. B. Duke and A. Bagchi, J. Vac. Sci. Technol (to be published).
[36]C. B. Duke, A. J. Howsmon, and G. E. Laramore, J. Vac. Sci. Technol. 8, 10 (1971).
[37]G. E. Laramore, C. B. Duke, A. Bagchi, and A. B. Kunz, Phys. Rev. B 4, 2058 (1971).
[38]G. E. Laramore and C. B. Duke, Phys. Rev. B 5, 267 (1972).
[39]C. B. Duke and U. Landman (unpublished).

PHYSICAL REVIEW B VOLUME 5, NUMBER 8 15 APRIL 1972

Correlation Potentials in a Nonuniform Electron Gas

K. J. Duff* and A. W. Overhauser
Scientific Research Staff, Ford Motor Company, Dearborn, Michigan 48121
(Received 17 December 1971)

A microscopic theory of the correlation operator, directed toward conduction electrons in a metal, is developed. The off-diagonal matrix elements, between electron states $\vec{k}$ and $\vec{k}+\vec{q}$, that arise when the electron density has a modulation of wave vector $\vec{q}$, determine the correlation contribution to band structure. These are computed explicitly. They depend dramatically on $\vec{k}$ (i.e., nonlocal behavior) and on $\vec{q}$. The sum of exchange and correlation operators is also nonlocal, but is less singular than either individually. An alternative division of exchange plus correlation into screened-exchange plus Coulomb-hole operators is made. It is shown that the (often ignored) Coulomb-hole operator is usually much larger than the screened-exchange operator.

I. INTRODUCTION

The contribution of exchange and correlation to one-electron Hamiltonians is a widely debated and important problem. Our attention here is focused on energy-band problems for crystalline solids. The periodic potential that appears in a (one-electron) Schrödinger equation must have contributions from exchange and correlation as well as from the Hartree term.

The exchange operator A^X is often replaced by the Slater $\rho^{1/3}$ approximation,[1]

$$A_S^X = -3e^2(3\rho/8\pi)^{1/3} \quad , \tag{1.1}$$

where $\rho(\vec{r})$ is the local electron density. It has been shown[2] that A_S^X is a very poor approximation to A^X. For band calculations the off-diagonal matrix elements of A^X arising from a spatial modulation of ρ (having, say, wave vector $\vec{q}$) are the most relevant quantities. Not only does $\langle\vec{k}+\vec{q}|A^X|\vec{k}\rangle$ depend markedly on $\vec{k}$, which shows that A^X is severely nonlocal, but it also depends on $\vec{q}$. For some combinations of $\vec{k}$ and $\vec{q}$ it is singular. In contrast Eq. (1.1) leads to off-diagonal matrix elements that are independent of $\vec{k}$ and $\vec{q}$.

Arguments which suggest approximations such as (1.1), or variants[3] of it, are supposedly most reliable for small q. It was therefore surprising to find[2] that the relevant off-diagonal elements of A^X become infinitely large in comparison with those obtained from the approximation (1.1) as $q \to 0$.

The sum of exchange and correlation operators, $A^{XC} \equiv A^X + A^C$, is of paramount physical interest. If A^{XC} is to be well behaved for $q \to 0$, then $\langle\vec{k}+\vec{q}|A^C|\vec{k}\rangle$ must become infinite (and have negative sign) relative to (1.1). This surmise[2] contrasts sharply with a very small and positive value suggested by prior work.[3]

The purpose of this study is to develop a *microscopic* theory of the correlation potential so that the explicit dependence of $\langle\vec{k}+\vec{q}|A^C|\vec{k}\rangle$ on $\vec{k}$ and $\vec{q}$ can be calculated. By combining this with the known[2] behavior of A^X, we determine the $\vec{q}$ dependence and nonlocal behavior of A^{XC}. This is carried out in Secs. II and III. The plasmon model[4] for treating dynamic correlations of electrons is employed. The off-diagonal behavior of A^C and A^{XC} in the $q \to 0$ limit is treated in Sec. IV.

The exchange and correlation operator can be subdivided into screened-exchange and Coulomb-hole operators, $A^{XC} \equiv A^{SX} + A^{CH}$. This alternative subdivision is displayed in Sec. V. We show that screened exchange is generally much less important than the Coulomb-hole potential. This deserves emphasis because the Coulomb-hole potential is often completely ignored. In some calculations its neglect can lead (and has led) to grossly incorrect conclusions.

II. FORMULATION OF CORRELATION OPERATOR

A microscopic theory of the correlation operator depends primarily on the excitation spectrum of the electron system. For a degenerate electron gas, this spectrum consists of plasma and single-particle excitations. The simplifying feature of the plasmon